



Assessing soil compaction risk: identifying the optimal measure of effective load in multi-pass conditions

Andre Peters , Kai Germer , Martin Kraft ^{*} , Marco Lorenz 

Thünen Institute of Agricultural Technology, Bundesallee 47, 38116 Braunschweig, Germany

ARTICLE INFO

Keywords:

Vertical soil displacement
Vertical soil deformation
Agriculture
Tyres
Wheel load

ABSTRACT

Soil compaction is a major challenge in modern agriculture. Multiple wheel passes with varying wheel types, sizes and loads are common, and the resulting impact on compaction remains unclear. This study aims to develop and evaluate a simple method to aggregate total wheel loads from multiple wheel passes to quantify their effect on soil compaction, disregarding other factors such as wheel size or type. From 2016 to 2021, 20 field trials were conducted on a silty loam site in northwest Germany, involving 1 to 8 wheel passes. For each wheel pass, static mass and vertical soil displacement at three depths were determined. Different aggregation schemes to calculate one effective load (L_{eff}) for all wheels were analyzed. A linear statistical model was applied to link vertical soil displacement to L_{eff} , soil depth, initial bulk density and water content. The best-performing scheme for L_{eff} closely matched the simple cumulative wheel loads (RMSE: 0.147 cm; r^2 : 0.59), while variants resembling maximum wheel load performed poorly (RMSE: 0.174 cm; r^2 : 0.43). All other variants lay between these two special cases. Our results suggest that for multiple wheel passes, the simple cumulative load is a reliable predictor for use in the assessment of soil compaction.

1. Introduction

Compaction affects many properties of soils and thereby impairs plant development and crop productivity (O'Sullivan and Simota, 1995). Therefore, preventing compaction may stabilize and/or increase yields and promote sustainability (Soane and van Ouwerkerk, 1994; Horn, 2003; Horn et al., 2006; Tullberg, 2010; McPhee et al., 2020; Duttman et al., 2022).

In agriculture and forestry, compaction is usually caused by field traffic, e.g., by harvest or manure application (Startsev and McNabb, 2001; Botta et al., 2009; Seehusen et al., 2019; Ten Damme et al., 2021; Germer et al., 2025). Compaction occurs when the applied soil stress exceeds the soil's precompression stress (both expressed as pressure) (Lebert and Horn, 1991; Horn and Peth 2011). The precompression stress depends on soil properties such as texture and bulk density, and on soil conditions such as moisture (Hamza and Anderson, 2005; Lamandé and Schjøning, 2011a; Schjøning and Lamandé, 2018, Ren et al. 2019), whereas the soil's stress depends on the wheel load, contact area of the wheels and also on soil properties and conditions (Söhne, 1958; Keller et al., 2002; Arvidsson and Keller, 2007; Lamandé et al. 2007; Horn and Fleige, 2009; Lamandé and Schjøning 2011b; Zink et al.,

2010). The underlying processes behind these effects are diverse and complex (Horn et al. 1995, Alakukku et al. 2003, Keller et al. 2013). Therefore, the prediction of compaction remains challenging since the required information for a certain event is often unavailable and thus several simplifying assumptions have to be made, regarding e.g., the homogeneity of both the soil properties and the soil conditions (Van den Akker, 2004; Keller et al., 2007).

Even more challenging is understanding the processes that occur during repeated wheeling (Horn et al. 2003; Peth et al., 2010; Mordhorst et al., 2012). Hence, empirical studies on this topic are of high importance. Lipiec et al. (1992) observed for example a linear relationship between the vertical deformation of plough layer soil and the logarithm of the number of wheel passes. Peth and Horn (2006) demonstrated, that even the first pass of a farm vehicle can result in deep reaching soil deformation, if the applied stresses exceed soil strength. From laboratory measurements, they described an exponential decrease with increasing number of cyclic loads. Even under light-weight traffic, crop yields were found to decrease with each additional wheel pass, highlighting the critical role of topsoil properties in supporting plant growth (Campbell et al., 1986). Ten Damme et al. (2021) found that the effects of repeated wheeling with a tractor-trailer combination on bulk density

* Corresponding author.

E-mail address: martin.kraft@thuenen.de (M. Kraft).

were well described by a linear model relating bulk density to the number of wheel passes. Patel and Mani (2011) experienced the same effect for a rather light wheel (0.84 t), where bulk density and penetration resistance increased unceasingly and linearly from pass 1 to 16 in the 15 cm to 30 cm depth zone. Majdoubi et al. (2024) found a decreasing impact of subsequent wheel passes on cone resistance for a very light field robot on a greenhouse soil which might not be representative for heavy agricultural traffic.

Cone penetration resistance increases linearly with the number of successive wheelings (Botta et al., 2009; Naderi-Boldaji et al., 2017; Patel and Mani, 2011), whereas Blackwell and Soane (1981) found a growing increase of cone resistance with four wheel passes on freshly ploughed, wet sandy loam. Zink et al. (2011) reported a significantly greater reduction in air-filled pore space in the subsoil (40–60 cm depth) after ten wheel passes compared to a single pass. Pulido-Moncada et al. (2019) observed that a single high wheel load (~12 t) had minimal impact on compaction at depths greater than 50 cm, whereas repeated

wheel passes with lower loads (~8 t) caused a comparatively greater effect at the same depth and site.

Most of the above-mentioned studies were conducted systematically with similar loads for each repeated wheeling. In real farming events, not only the number, size and inflation pressure of wheels differ but also the load of each wheel (e.g., Germer et al., 2025), which makes the interpretation even more complicated. Under such conditions, it is not clear how to calculate the effective load after a harvesting or fertilizer application event. In order to evaluate the impact of multiple wheeling on the water retention characteristics, Germer et al. (2025) introduced a weighted cumulative load to address this question. However, their approach is solely conceptual and was not tested or compared with other possible approaches. We note that a reliable measure for the effective load for multiple wheel passes is a prerequisite for moving away from the idealized consideration of a single wheel and including the multiple wheel passes that are common in agricultural practice in the assessments of the soil compaction risk.

Table 1

List of all 20 performed wheeling trials, with the corresponding trial conditions. θ and ρ_b are the volumetric water contents and bulk densities of the reference pits.

#	Campaign (year/month) abbreviation	Description	Load for each wheel								θ			ρ_b		
			[kg]								[cm ³ cm ⁻³]			[g cm ⁻³]		
			1	2	3	4	5	6	7	8	20 cm	35 cm	50 cm	20 cm	35 cm	50 cm
1	digestate application (2017/03) da17	Self-propelled slurry tank (crab steering)	10,000								0.35	0.32	0.33	1.50	1.53	1.50
2		Self-propelled slurry tank (multi-pass)	10,000	10,900												
3		Tractor plus tandem slurry tank	1600	4300	4600	3800										
4		Tractor with umbilical cord technique	1700	4300												
5	digestate application (2019/03) da19	Self-propelled slurry tank (crab steering)	10,580								0.36	0.36	0.36	1.45	1.48	1.49
6		Self-propelled slurry tank (multi-pass)	10,580	10,110												
7		Tractor plus tandem slurry tank	1640	3860	3600	3430										
8		Tractor plus tridem slurry tank	2820	5570	6200	6270	5600									
9		Tractor with umbilical cord technique	1900	4640												
10	digestate application (2021/03) da21	Self-propelled slurry tank (crab steering)	9830								0.35	0.37	0.37	1.49	1.48	1.46
11		Tractor plus tandem slurry tank	1060	2990	4400	4320										
12		Tractor plus tridem slurry tank	2760	6340	4960	6060	5890									
13		Tractor with umbilical cord technique	1900	4640												
14	harvest sugar beet (2016/10) sb16	Beet harvester (full)	10,380	9740	10,060				0.34	0.25	0.14	1.42	1.50	1.49		
15		Beet harvester (half full)	8590	7275	7960											
16	harvest sugar beet (2019/10) sb19	Beet harvester (crab steering, full)	11,180								0.33	0.33	0.35	1.44	1.49	1.43
17		Beet harvester (crab steering, half full)	9280													
18	harvest silage maize (2017/10) sm17	Harvesting chain (chopper, tractor + silo trailer, tractor + mulcher)	7140	2470	2200	3730	4820	4870	1725	1800	0.38	0.36	0.34	1.48	1.55	1.51
19		Tractor plus silo trailer	2200	3730	4820	4870										
20	harvest winter wheat (2017/08) ww17	Combine harvester (full)	6450	2005							0.38	0.38	0.38	1.31	1.47	1.48

*no data available.

The aim of this study is to find the best approach for calculating the effective load of multiple wheel passes for real farm conditions, requiring only limited information. For this, we generalized the approach of Germer et al. (2025) and applied a linear statistical model to link soil vertical displacement as measure for compaction to soil depth, bulk density, water content and several expressions of effective load.

2. Material and methods

2.1. Study site

The study was conducted on a stagnic Luvisol near the village of Adenstedt (268 m above sea level) in southern Lower Saxony, Germany (52°00'18.6"N, 9°56'31.4"E). The average sand, silt, and clay contents in the topsoil (0–30 cm) were 2%, 80%, and 18%, respectively, while in the subsoil (>30 cm), they were 2%, 77%, and 21%. Soil organic carbon content was approximately 1.2% in the topsoil and 0.3% in the subsoil (Kuhwald et al., 2016). The soil texture class was classified as silt loam for both depths.

2.2. Wheeling events

From 2016 to 2021, seven measurement campaigns were conducted to investigate the effects of various wheel loads on soil compaction. These campaigns included three digestate application campaigns, two sugar beet harvest campaigns, one silage maize harvest campaign, and one winter wheat harvest campaign. Each campaign involved multiple wheeling events, varying the harvest or digestate application system and techniques, resulting in a total of 20 distinct trials. Table 1 gives an overview of the 20 trials with the single wheel loads as well as the volumetric water contents and bulk densities of the unwheeled areas. Contact area and contact area pressure, which are not part of the model developed (see below), are documented for informative purposes in the supplement S1. More details about the study site and the experimental

conditions concerning the wheeling and soil sampling can be found in Peters et al. (2025) and Germer et al. (2025).

2.3. Measurements

2.3.1. Basic soil measurements

For each campaign, one (sb19 and ww17) or two (all others) reference pits were dug at unwheeled places, and 5 undisturbed soil samples were taken in 100 cm³ cores at depths of 20, 35 and 50 cm in each pit. Immediately after sampling, the soil cores were weighed with an accuracy of 0.01 g, subsequently oven-dried at 105 °C for at least 24 h and again weighed to determine the dry bulk density (ρ_b) [g cm⁻³] according to DIN ISO 11272:2001–01 and the initial volumetric water content (θ) [cm³ cm⁻³] according to DIN ISO 11465 at field conditions. Their mean values are given in Table 1.

2.3.2. Measurement of vertical soil displacement

Vertical soil displacement was measured with a self-constructed multi-channel device described by Nolting et al. (2006), which operates based on a hydrostatic water column. Basically, the system relies on communicating tubes, with one end fixed to a pressure sensor as a reference level and the open end acting as a probe to measure height differences (Δh) relative to the water meniscus of the water column (Fig. 1A). To eliminate the influence of ambient air pressure, a “tube-in-tube” system is operated. It consists of an inner open water-filled tube enclosed within a sealed outer tube. A differential pressure transducer measures the pressure difference between the tubes, creating a closed system that prevents water loss. In order to guarantee a stable pressure on the air side of the differential pressure transducer, the pressure in the air space between the water tube end and the outer tube (p_{air}) must be equal to or greater than atmospheric pressure (p_{atm}). The outer air-filled polyamide tube (inner diameter: 0.4 cm) acts as a protective cover, while the inner tube (0.1 cm) contains the water. To prevent pressure transmission errors from air bubbles, degassed water is used. The outer

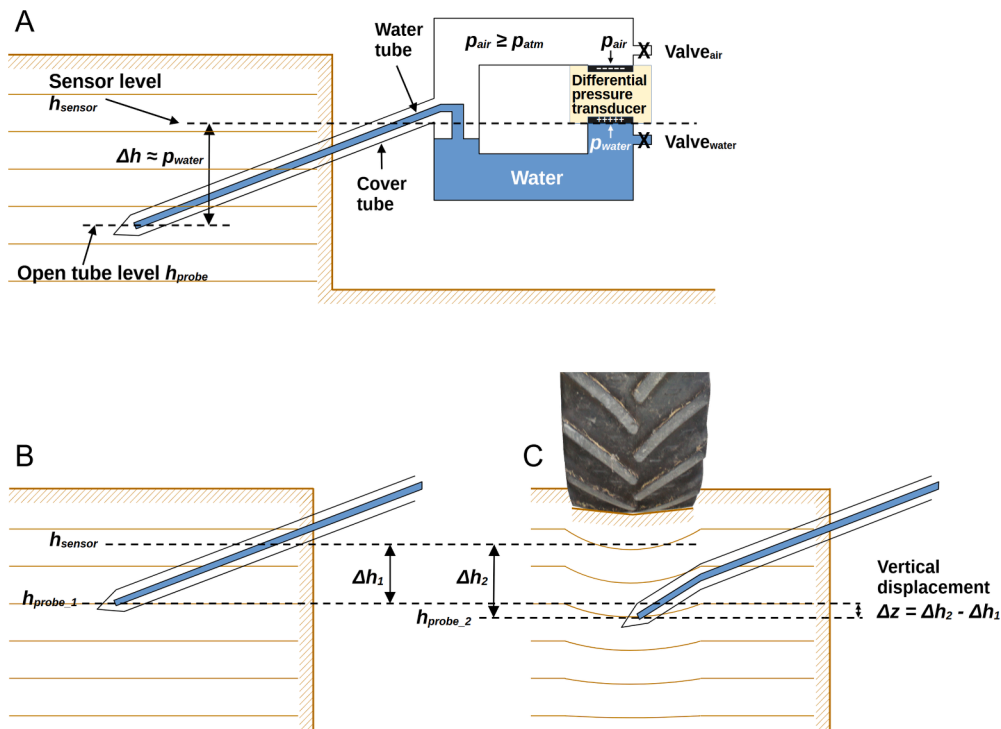


Fig. 1. Measurement principle of vertical displacement. A: Schematic of the „tube in tube” system. The pressure of the water column (p_{water}), which equals the difference in height (Δh) between the end of the water-tube at the pressure transducer and the end of the open tube; B: Installed pressure tube before wheeling. C: Vertical displacement of soil and pressure tube tip during and after wheeling. Δz indicates the change of depth for the open end of the water pressure tube in case of vertical deformation downward.

tube adapts to soil movement, and a specialized fitting facilitates refilling and operation in the field.

The hydrostatic water column functions as a hanging column, where 1 mbar of water pressure equals approximately 0.1 cm in height of the water column. When the probe moves with soil displacement (Δz) due to loading, Δh changes accordingly, representing vertical displacement by $\Delta h_2 - \Delta h_1 = \Delta z$ (Fig. 1B and 1C). The resolution of the displacement measurement is 0.01 cm.

Soil pressure was also measured by using self-constructed Bolling probes according to Bolling (1985, 1987), which consist of a water-filled pipe with a flexible 10 cm silicone hose at the end. To ensure soil contact, an initial water pressure of 1.0 bar was applied. Soil pressure data were not used for modelling in this study. They are shown for information purpose in Fig. 3 and Figs. S1 to S20 Supplement .

The multi-channel system included three displacement probes at 20 and 35 cm depths and two at 50 cm for repeated measurements, whereas pressure probes were installed in triplets in the same three depths. All probes were installed in pre-drilled boreholes (12° angle) directly under the tire track (Fig. 2A). The spatial arrangement of measurement points is shown in Fig. 2B. The measured values were logged in an interval of 0.016 s.

2.4. Evaluation

2.4.1. Evaluation of soil displacement measurements

A pre-processing step was performed to (i) exclude malfunctioning probes and (ii) account for the time lag in the signals. The latter was necessary because the probes at each depth were spaced 12 to 60 cm apart, causing their signals for a single wheel to be delayed by approximately 0.1 to 0.5 s, depending on the probe distance and the velocity of the machinery. Since the absolute timestamps of the signals were irrelevant, we consistently used the time of a distinct peak in the first pressure probe as the reference. For the other probes, we identified the corresponding peak times for both pressure and displacement probes and shifted their entire time series by the determined time lag.

After pre-processing, the mean vertical plastic soil displacement after each wheel had to be determined. Since the displacement measurements oscillated during wheeling, the mean displacement for the repetitions was calculated within a 0.25-second interval (including 15 logged values), starting 1 s before the pressure peak of the succeeding wheel. This interval had to begin at least 1 s after the preceding pressure peak. After the last wheel, the time lag was set to 5 s. We refer to these valid time intervals as “valid 1”. Fig. 3 exemplarily shows this for the digestate application 2019 with a tractor with tridem slurry tank (Table 1, # 8), i. e., with 5 wheel passes.

When the time between two single wheels to pass a given probe was below 2 s (e.g., for a specific machine or tractor), we placed the 0.25-second interval at the midpoint between the neighboring peaks. In such cases, we visually inspected the validity of the mean displacement by analyzing the oscillations in the probe signals. The valid values are labeled as “valid 2,” while the invalid ones are labeled as “invalid” (Fig. 3). Finally, the mean for the valid repetitions was calculated for each depth. The according figures for all 20 wheeling events are shown in the Supplemental materials (Figs. S1 to S20). Each valid displacement was used as response for the modelling described below. The valid displacement data sum up to 123, i.e., 41 measurement times (20 values at the end of each event and 21 values between single wheels) and 3 depths.

2.4.2. Effective load

There is still no clear solution for addressing the cumulative effect of multiple wheel passes—differing in type, inflation pressure and load—on soil compaction, nor for defining an effective load under such conditions. Germer et al. (2025) defined the effective cumulative load for a scenario of consecutive wheeling with varying loads by assuming that the highest wheel load exerts the greatest impact on soil

compaction, while lower loads have progressively diminished effects. Therefore, they first sorted the individual wheel loads in descending order, starting with the highest load. Then they calculated the cumulative effective wheel load L_{eff} [kg] by:

$$L_{\text{eff}} = \sum_{i=1}^k \frac{1}{i} L_i \quad (1)$$

where k [-] is the total number of wheels, and L_i [kg] is the load of the i th wheel (in descending order of the load). We generalize this heuristic approach by introducing what we call the extinction parameter n [-]:

$$L_{\text{eff}} = \sum_{i=1}^k \frac{1}{i^n} L_i \quad (2)$$

For $n = 0$, L_{eff} is the simple cumulative load, for $n = \infty$, L_{eff} equals the maximum wheel load, assuming that all less heavy wheels have no additional impact and for $L_{\text{eff}} = 1$, Eq. (2) equals the approach of Germer et al. (2025). For $n < 0$, the lighter wheels are attributed to a greater effect. In this study, we vary the value of n from -1 to 10 to find the best scheme for L_{eff} calculation (Fig. 4). In the variant with $n = 10$, L_{eff} equals approximately the maximum load, since the load of the second wheel is already weighted with $1/2^{10}$. For each n , L_{eff} was calculated for all 20 wheeling trials as well as for the valid vertical displacement between the wheels, resulting in 41 values of L_{eff} per n . For trial # 8 (Fig. 3), for example, three values for L_{eff} could be determined per n .

2.4.3. Statistical modelling

We used the vertical displacement of the soil (Δz [cm]) at the three depths as response and the effective Load (L_{eff} [kg]), the depths (z [cm]) as well as the volumetric water contents (θ [cm³ cm⁻³]) and bulk densities (ρ_b [g cm⁻³]) of the uncompacted soils as predictor variables and implemented a linear model with interactions. For the final displacement, L_{eff} was calculated based on all wheel loads, whereas for the valid displacement between the wheels, L_{eff} was based on the loads of the already passed wheels. Since the different predictors vary greatly by their order of magnitude, we scaled them by their maximum values:

$$x' = \frac{x}{x_{\text{max}}} \quad (3)$$

where x is the predictor or an interaction term, x_{max} is their maximum value, and x' is the transformed value. Since in our scenarios, vertical soil displacement (Δz [cm]) can only occur due to external forces, i.e., wheeling, we included only the effect of L_{eff} and interactions of the other predictors with L_{eff} . Moreover, to keep it simple, we included only linear interaction terms, leading to:

$$\Delta z = \beta_1 L'_{\text{eff}} + \beta_2 (\rho_b L'_{\text{eff}})' + \beta_3 (z L'_{\text{eff}})' + \beta_4 (\theta L'_{\text{eff}})' \quad (4)$$

where β_1 to β_4 are the model parameters to be estimated. In order to estimate only the significant interactions, we performed an automated backward selection, successively excluding parameters with a p-value > 0.05 until no remaining parameters had a p-value > 0.05 .

The model performance was evaluated using the coefficient of determination (r^2), the root mean squared error (RMSE) and the Akaike Information criterion (AIC). The latter accounts not only for the goodness of fit but also for the number of estimated parameters, which is important since the backward selection might eliminate different numbers of parameters. The adjustment of the linear models and the calculation of the corresponding statistical measures were performed using the Ordinary Least Squares (OLS) method, with the statsmodels library in Python (Seabold & Perktold, 2010).

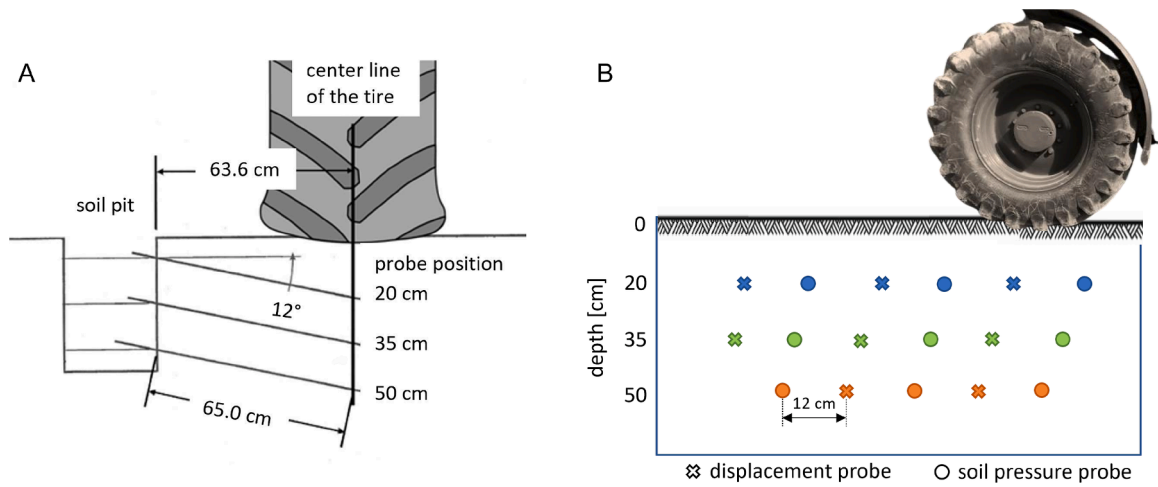


Fig. 2. Schematic of probe installation (A, front view) and spatial distribution of displacement and pressure probes from side (B, side view).

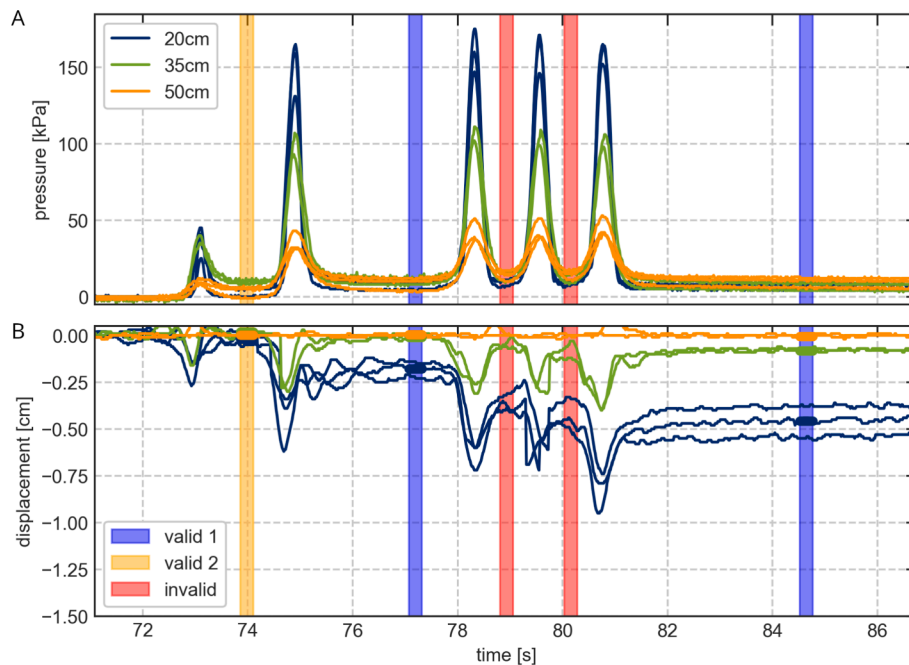


Fig. 3. Dynamic soil pressure (A) and vertical displacement (B) measured in the wheeling event for digestate application in March 2019 with a tractor with tridem slurry tank (# 8 in Table 1). “valid 1” and “valid 2”: calculated means of plastic displacement (thick short lines) used for further evaluation; “invalid”: calculated means of plastic displacement not used due to oscillation. Each pressure peak indicates a certain wheel pass.

3. Results and discussion

3.1. Correlation analysis

Fig. 5 shows the pair plot of vertical soil displacement (Δz) and the four predictors for $n = 0$, where L_{eff} represents the effective load. The correlations among the predictors are generally low. The highest correlation is observed between depth (z) and bulk density, with a correlation coefficient of 0.26. The correlation between Δz and the individual predictors is also relatively low, except for Δz versus z , which shows a correlation coefficient of 0.56. The relationship between Δz and L_{eff} is moderately negative, with a correlation coefficient of -0.39 . For $n = 1$ (L_{eff} representing the weighted load after Germer et al. (2025)) and $n = 10$ (L_{eff} approaching the maximum load), the correlation between Δz and L_{eff} is even smaller, with correlation coefficients of -0.36 and -0.27 , respectively (not shown).

3.2. Model analysis

The fitted (with Eq. (4) versus measured displacements are shown in Fig. 6 for three special values of n in Eq. (2), namely $n = 0$, $n = 1$ and $n = 10$. For all three variants, the backward elimination eliminated one to two of the 4 parameters in Eq. (4), leading to $\Delta z = \beta_1 L'_{eff} + \beta_3 (z L'_{eff})' + \beta_4 (\theta L_{eff})'$ and to $\Delta z = \beta_1 L'_{eff} + \beta_3 (z L'_{eff})'$, i.e., the initial bulk density had no significant impact, which is surprising. We attribute this to the relatively high variability in the measured initial bulk densities (Fig. 5) and the fact that the initial bulk densities and water contents were measured in one or two reference pits per campaign and hence might not perfectly represent the initial values at the exact locations of the trials. The initial bulk densities ranged between 1.31 and 1.55 g cm^{-3} , whereas the initial volumetric water contents range from 0.14 to 0.38 (Fig. 5). Interestingly, the variant with $n = 0$, i.e., when L_{eff} represents simply the cumulative load of all wheels, performs best,

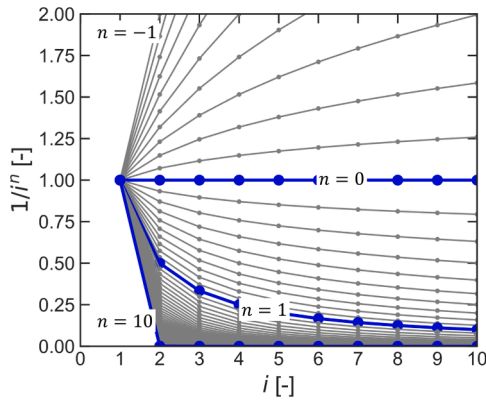


Fig. 4. Representation of weighing schemes ($\frac{1}{i^n}$ in Eq. (2)) for calculating different effective loads L_{eff} for 10 single wheel passes (i) sorted from the heaviest to lightest. Parameter n is varied from -1 (top line) to 10 (bottom line). The thick blue lines indicate three special cases, namely $n = 0$, $n = 1$ and $n = 10$ (i.e., $n \approx \infty$). (For interpretation of the references to colour in this figure legend, the reader is referred to the web version of this article.)

whereas the variant, which represents solely the wheel with the maximum load $n = 10$ performed worst (Fig. 6). Especially, the measured strong displacements in the 20 cm depths (the left-most points) were better described using $n = 0$. These model results are in line with the correlations between Δz and the different formulations of L_{eff} . There is no influence of either bulk density (colors of markers) or magnitude of L_{eff} (size of markers) on model performance.

Fig. 7 displays the statistical measures for the complete span of applied values for n for calculating L_{eff} . The best performance (highest r^2 or lowest RMSE and AIC) was found at $n = 0$. The estimated parameters as well as their back-transformed counterparts are displayed in Table 2. We note that the best RMSE is relatively large with 0.147 cm compared to the assumed measurement resolution of 0.01 cm. To ensure that our result is not due to the selected model, we also conducted this evaluation without backward selection, allowing all 4 model parameters of Eq. (4) in the final model. The resulting curves for the three statistical measures are almost identical (Fig. A1) with slight increase of model performance according to r^2 und RMSE. The optimum value for n is $n = -0.1$. In a last step, we allowed a variety of non-linear interactions, using the following model:

$$\Delta z = \beta_1 L'_{\text{eff}} + \beta_2 (\rho_b L'_{\text{eff}})' + \beta_3 (z L'_{\text{eff}})' + \beta_4 (\theta L'_{\text{eff}})' + \beta_5 (\sqrt{\rho_b} L'_{\text{eff}})' + \beta_6 (\sqrt{z} L'_{\text{eff}})' + \beta_7 (\sqrt{\theta} L'_{\text{eff}})' + \beta_8 (\rho_b^2 L'_{\text{eff}})' + \beta_9 (z^2 L'_{\text{eff}})' + \beta_{10} (\theta^2 L'_{\text{eff}})' \quad (5)$$

The resulting statistical measures are shown for both applying and not applying backward selection in Fig. A2. Again, the optimum value for n is close to 0.0 (the exact value is 0.1). Hence, the selected optimum value for n is most likely independent of the selected model complexity.

The model given by Eq. (5) has very high multicollinearity with variance inflation factors (VIF) from 143,250 to infinite.¹ Reducing multicollinearity by iteratively removing the term with highest VIF showed that high multicollinearity persists as long, as more than one term stays included for the same physical factor (ρ_b , z , and θ). The highest predictive potential with only one term per factor and modest multicollinearity could be achieved with this model:

¹ Calculated using python statsmodels.stats.outliers_influence.variance_inflation_factor.

$$\Delta z = \beta_1 (\sqrt{\rho_b} L'_{\text{eff}})' + \beta_2 (\sqrt{z} L'_{\text{eff}})' + \beta_3 (\theta^2 L'_{\text{eff}})' \quad (6)$$

This model gave only very little improvement over the linear model (Eq. 4) with an RMSE of 0.144 cm (Fig. A3), that still remains more than an order of magnitude higher than the measurement resolution. This suggests that the uncertainty in the measured data is not solely due to measurement errors but also influenced by additional factors beyond load, water content, depth, and bulk density—such as soil heterogeneity. This is also supported by the spread of the Δz data in one trial and depth, which is of a similar magnitude as the RMSE (see, for example, Fig. 3 or Figs. S1–S20 in the Supplemental materials). Due to the probable uncertainties in the measured data, we abstained from testing more non-linear models or interactions. The intention of this study was to find a simple empirical model to summarize variable wheel loads in a multi-pass event into a representative single effective load L_{eff} for practical assessment of compaction and vertical displacement.

In this study, soil conditions, i.e. initial ρ_b and θ were determined by real farm conditions and time restrictions. A more widespread range of initial ρ_b (pre-stress) and θ is desirable for statistical stability and trustworthiness of the model in future studies. Consideration of contact area, contact area pressure or tyre width may also improve the model outcome in future studies, but such data are often not available.

Summarizing, the exact value of n was always very close to 0. Given the large variability in the data and model uncertainties, setting n to 0 is, in our view, justified. Our exponential approach and the optimization of the extinction parameter n lead to the simple cumulative calculation of L_{eff} ($n = 0$). Hence, the simple cumulative load is an appropriate predictor for assessing compaction risk under real farm conditions on a silty Luvisol, whereas the usage of only the maximum load or the weighted load as suggested by Germer et al. (2025) cannot be recommended.

Compaction effects in a linear relationship to the number of wheel passes were already observed in previous studies: Ten Damme et al. (2021) found a good linear relationship between number of up to six wheel passes and bulk density. Botta et al. (2009) found a linear relationship between cone index and number of tractor passes for up to five (0–200 mm depth range) resp. ten (200–400 mm and 400–600 mm) passes. Other studies found a linear relation between observed compaction effects and the logarithm of the number of wheel passes (eg. Lipiec et al., 1992; Peth and Horn, 2006; Peth et al., 2010; Mordhorst et al., 2012). Like the before-mentioned studies of Ten Damme et al. (2021) and Botta et al. (2009), our study was based on real farm oper-

ations with one to eight wheel passes, taking into account a wide variety of wheel loads within one passage (Tab. 1). Obviously, vertical soil deformation cannot be linearly correlated to an *unlimited* number of passes, and the model is not suited for an arbitrary large number of wheel passes.

The experiment was carried out on a very silty Luvisol (80% silt). Pytka (2005) and Pytka et al. (2006) emphasized the complex deformation properties of loess soil as compared to a sandy soil due to the cohesion and aggregate structure of loess soil. The elastic properties of the soil are obvious after each wheel pass in Fig. 3. It must be emphasized that the linearity found in this study is related to the vertical displacement, not to bulk density or cone index. The specific approach of this study was to use the vertical deformation Δz to describe the compression of the soil, because our apparatus (Fig. 1) allowed the measurement of Δz after each single wheel pass, such increasing the number of observations from 20 to 41 measurements. Further studies

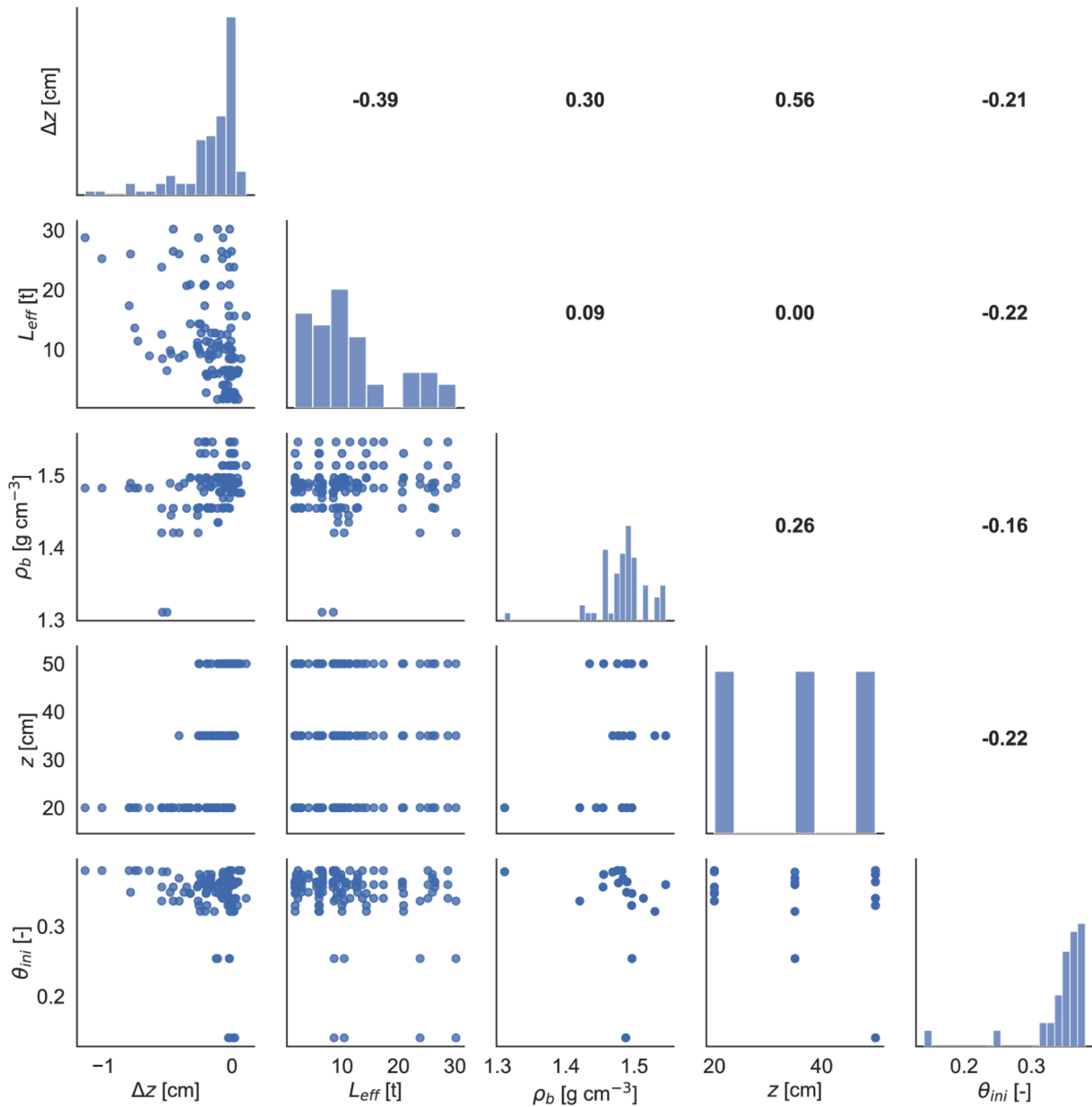


Fig. 5. Pair plot of vertical soil displacement (Δz) and the four predictors. The parameter n in Eq (2) was 0, i.e., L_{eff} is the simple cumulative load. The numbers in the plots indicate the Pearson correlation coefficients.

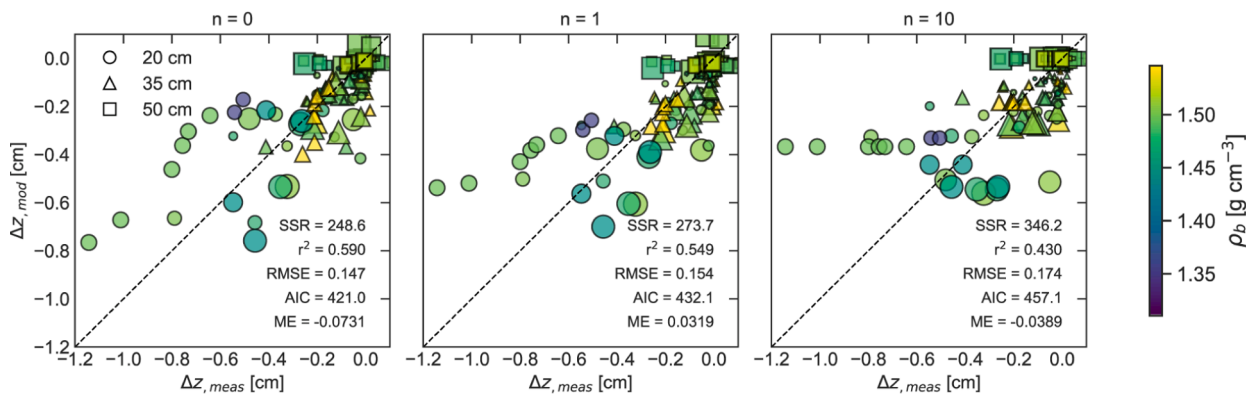


Fig. 6. Comparison of measured and modeled soil displacements in the three soil depths for three different values of n in Eq (2). Left: $n = 0$ (i.e., L_{eff} is simply the cumulative load); center: $n = 1$ (i.e., L_{eff} according to Germer et al., 2025); right: $n = 10$ (i.e., L_{eff} equals approximately the maximum wheel load). The size of the markers indicates the magnitude of L_{eff} .

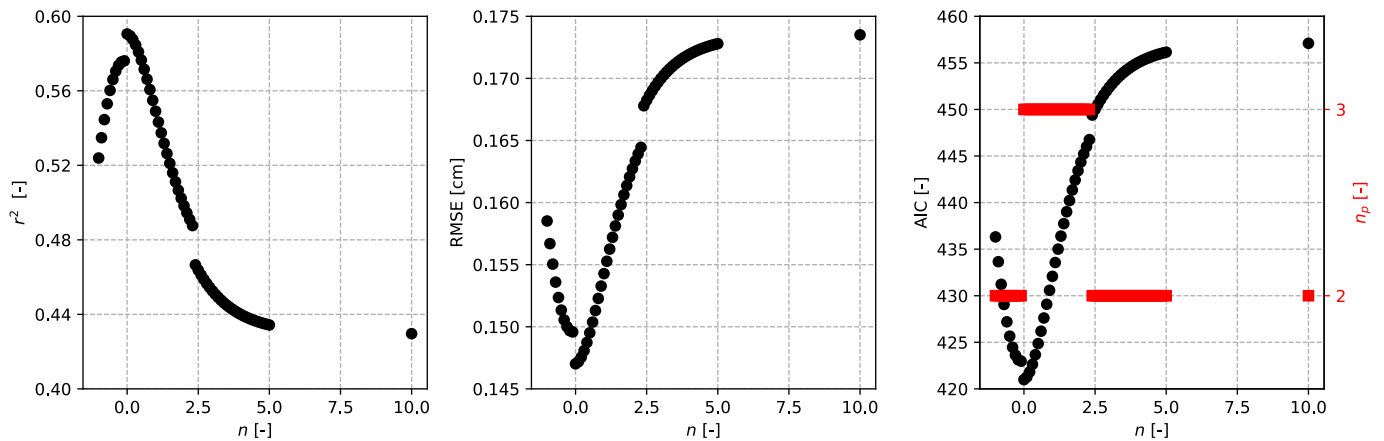


Fig. 7. Statistical measures for the different values of L_{eff} in Eq. (2) using the simple statistical model Eq. (4). n_p indicates the number of remaining fitted parameters after backward selection.

Table 2

Scaling factors and estimated regression coefficients of the model (Eqs. (3,4), with the optimal extinction parameter $n = 0$). (*): p-value < 0.05, (**): p-value < 0.001, (***): p-value < 0.0001.

	L_{eff}	$\rho_b L_{eff}$	$z L_{eff}$	θL_{eff}
Unit	[kg]	[g cm ⁻³ kg]	[cm kg] (depth z given as positive value)	[cm ³ cm ⁻³ kg]
x_{max}	3.018×10^4	4.517×10^4	1.5090×10^6	1.0920×10^4
β value	β_1 [cm kg ⁻¹] -8.942***	β_2 [cm g ⁻¹ cm ³ kg ⁻¹]	β_3 [cm cm ⁻¹ kg ⁻¹] 12.155***	β_4 [cm cm ⁻³ cm ³ kg ⁻¹] -3.767*
$\frac{\beta}{x_{max}}$	-2.963×10^{-4}	-	8.055×10^{-6}	-3.449×10^{-4}

may also consider to determine bulk density and/or cone index changes after the wheeling event. The general applicability of our results with respect to n , and the influence of soil type on the effects of multi-pass events should be investigated in future comparative work on different soil types.

The predicted vertical soil displacement as function of L_{eff} (calculated with $n = 0$) and volumetric water content is shown in Fig. 8. We used Eq. (4) with the parameters given in Table 2. Compaction increases with both increasing L_{eff} and increasing water content. Note that the model does not predict a certain threshold for displacement as it is linear in all aspects. However, it might help to understand the general

vulnerability of the site due to effective load and soil water content. With relatively high water contents ($\theta = 0.4$), the soil might be compacted in the subsoil which is critical.

4. Summary and conclusion

We developed a general scheme to calculate the effective load (L_{eff}) for multiple wheelings with different single-wheel loads, assuming only the static load of the individual wheels is known. This conceptual scheme includes one unknown parameter, which we call the extinction parameter (n). Two special cases are of particular interest: for $n = 0$, L_{eff}

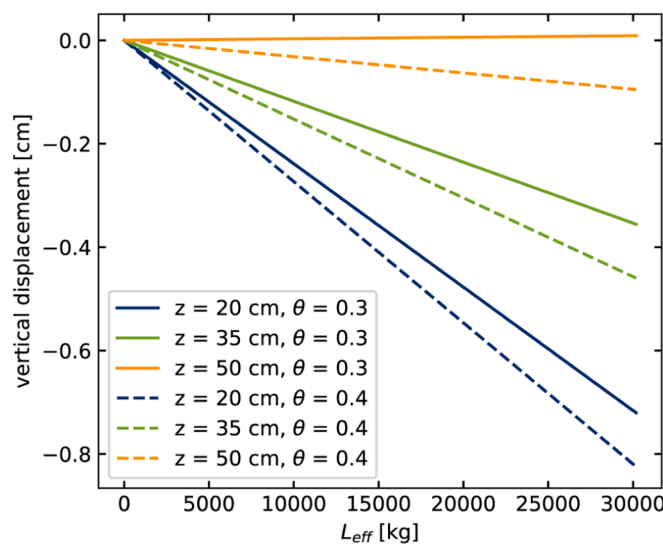


Fig. 8. Modelled vertical displacement with fitted Eq. (4) as function of depth, volumetric water content (θ) and L_{eff} with $n = 0$.

is the simple cumulative load, and for $n = \infty$, L_{eff} equals the maximum wheel load.

We used a large data set consisting of several different wheeling events on a real farm, with varying numbers of wheels and wheel loads, to find the optimum value for n . The measured vertical soil displacement at three depths was used as the response variable, with effective loads, volumetric water contents, bulk densities, and soil depths as predictor variables. A simple linear model was fitted to the data with varying values for n .

Based on our comprehensive data set, the variant expressing the maximum wheel load performed the worst, whereas the best estimate was obtained for $n = 0$. Therefore, we conclude that the impact of the load on soil compaction in the case of multiple wheelings is well assessed using the cumulative load of all wheels (i.e., $n = 0$). This result was consistent across different models. We note that our findings are based on data from only four fields with stanic Luvisol, meaning their transferability to other sites with different soil condition must be tested.

Funding information

This research was conducted within the SOILAssist project that was funded by the Federal Ministry of Education and Research (BMBF), Germany, within the framework of the BonaRes-initiative (grants no. 031A563A, 031B0684A and 031B1065A).

CRedit authorship contribution statement

Andre Peters: Writing – original draft, Visualization, Validation, Software, Methodology, Conceptualization. **Kai Germer:** Writing – review & editing, Data curation, Conceptualization. **Martin Kraft:** Writing – review & editing, Validation, Conceptualization. **Marco Lorenz:** Writing – review & editing, Project administration, Investigation, Funding acquisition, Conceptualization.

Appendix

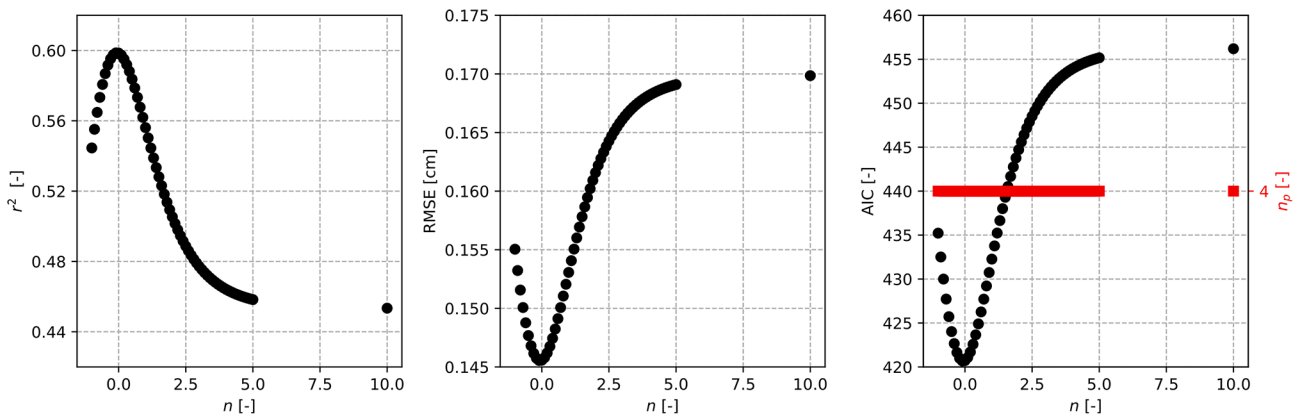


Fig.A1. Statistical measures for the different values of n in Eq. (2) without using backward selection, i.e., allowing all 4 parameters in Eq. (4) to be fitted.

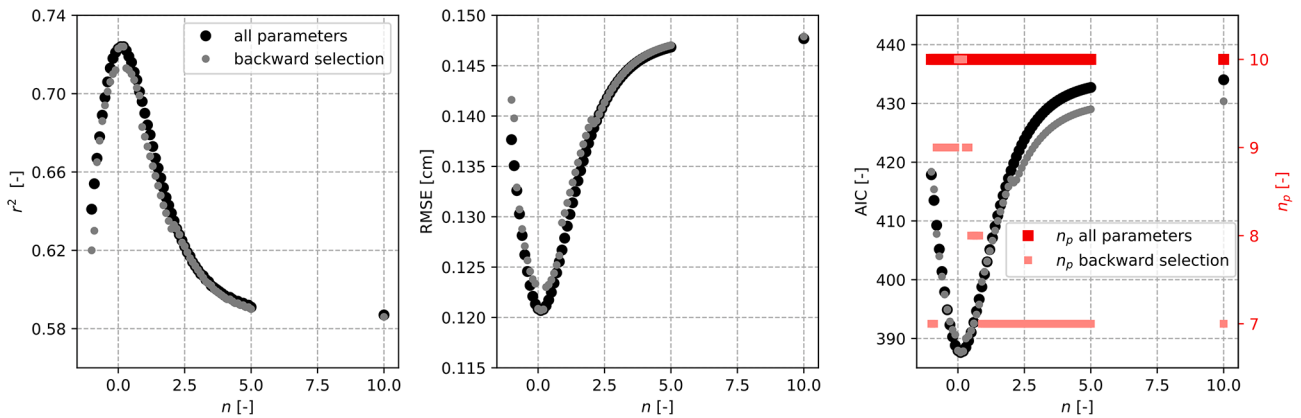


Fig.A2. Statistical measures for the different values of n in Eq. (2) using the flexible statistical model (Eq. (5) with and without applying backward selection). n_p : number of fitted parameters.

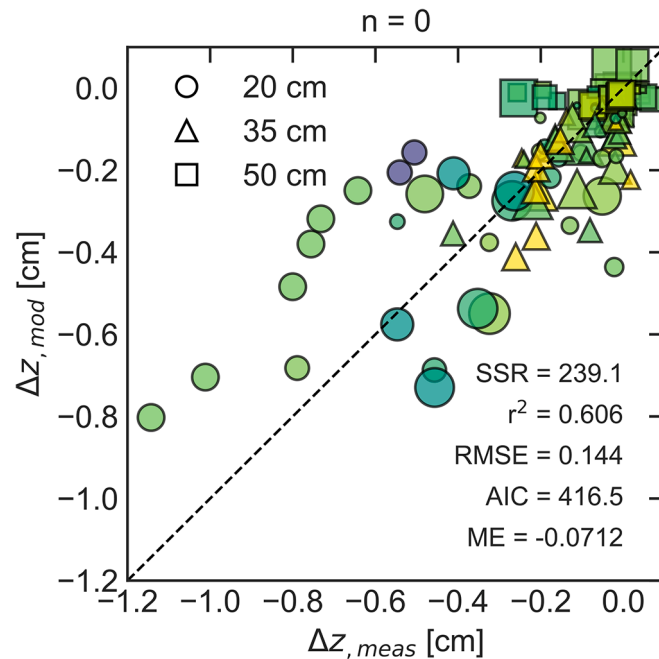


Fig. A3. Comparison of measured and modeled soil displacements in the three soil depths with $n = 0$ and the model of Eq. (6). For details of the graph, refer to Fig. 6.

Appendix A. Supplementary material

Supplementary data to this article can be found online at <https://doi.org/10.1016/j.jterra.2026.101125>.

References

- Alakukku, L., Weisskopf, P., Chamen, W.C.T., Tijink, F.G.J., van der Linden, J.P., Pires, S., Sommer, C., Spoor, G., 2003. Prevention strategies for field traffic-induced subsoil compaction: a review. Part 1: machine/soil interactions. *Soil Tillage Res.* 73 (1–2), 145–160.
- Arvidsson, J., Keller, T., 2007. Soil stress as affected by wheel load and tyre inflation pressure. *Soil Tillage Res.* 96, 284–291.
- Blackwell, P.S., Soane, B.D., 1981. A method of predicting bulk density changes in field soils resulting from compaction by agricultural traffic. *Eur. J. Soil Sci.* 32, 51–65. <https://doi.org/10.1111/j.1365-2389.1981.tb01685.x>.
- Bolling, H.L., 1985. How to predict soil compaction from agricultural tires. *J. Terramechanics* 22 (4), 205–223. [https://doi.org/10.1016/0022-4898\(85\)90017-5](https://doi.org/10.1016/0022-4898(85)90017-5).
- Bolling, I., 1987. Bodenverdichtung und Triebkraftverhalten bei Reifen - Neue Meß und Rechenmethoden (Doctoral dissertation, Lehrstuhl für Landmaschinen, Techn. Univ.).
- Botta, G.F., Becerra, A.T., Tourn, F.B., 2009. Effect of the number of tractor passes on soil rut depth and compaction in two tillage regimes. *Soil Tillage Res.* 103 (2), 381–386.
- Campbell, D.J., Dickson, J.W., Ball, B.C., Hunter, R., 1986. Controlled seedbed traffic after ploughing or direct drilling under winter barley in Scotland, 1980–1984. *Soil Tillage Res.* 8, 3–28.
- Duttmann, R., Augustin, K., Brunotte, J., Kuhwald, M., 2022. Modeling of field traffic intensity and soil compaction risks in agricultural landscapes. In: *Advances in Understanding Soil Degradation*, pp. 313–331. Springer, Cham.
- Germer, K., Shafiullah, A.Z., Peters, A., Kraft, M., Weise, M., Rolfes, L., Lorenz, M., 2025. Field traffic loads on a silty farm site cause shifting and narrowing of soil pore size distribution. *Soil Tillage Res.* 248, 106425.
- Hamza, M.A., Anderson, W.K., 2005. Soil compaction in cropping systems: a review of the nature, causes and possible solutions. *Soil Tillage Res.* 82, 121–145. <https://doi.org/10.1016/j.still.2004.08.009>.
- Horn, R., Domzal, H., Slowinskajurkiewicz, A., van Ouwerkerk, C., 1995. Soil compaction processes and their effects on the structure of arable soils and the environment. *Soil Tillage Res.* 35 (1–2), 23–36. [https://doi.org/10.1016/0167-1987\(95\)00479-C](https://doi.org/10.1016/0167-1987(95)00479-C).
- Horn, R., 2003. Stress-strain effect in structured unsaturated soils on coupled mechanical and hydraulic processes. *Geoderma* 116, 77–88. [https://doi.org/10.1016/S0016-7061\(03\)00095-8](https://doi.org/10.1016/S0016-7061(03)00095-8).
- Horn, R., Way, T.R., Rostek, J., 2003. Effect of repeated tractor wheeling on stress/strain properties and consequences on physical properties in structured arable soils. *Soil Tillage Res.* 73, 101–106. [https://doi.org/10.1016/S0167-1987\(03\)00103-X](https://doi.org/10.1016/S0167-1987(03)00103-X).
- Horn, R., Fleige, H., Peth, S., Peng, X. (Eds.), 2006. *Soil management for sustainability. Advances in Geocology* 38. Catena Verlag, Reiskirchen, Germany, ISSN (Print): 0722-0723.
- Horn, R., Fleige, H., 2009. Risk assessment of subsoil compaction for arable soils in Northwest Germany at farm scale. *Soil Tillage Res.* 102 (2), 201–208.
- Horn, R., Peth, S., 2011. Mechanics of unsaturated soils for agricultural applications. In: Huang, P.M., Li, Y., Sumner, M. (Eds.), *Handbook of Soil Sciences*, 2nd ed., chap. 3, pp. 1–30. Taylor and Francis. ISBN: 978-1-4398-0305-93-14.
- Keller, T., Trautner, A., Arvidsson, J., 2002. Stress distribution and soil displacement under a rubber-tracked and a wheeled tractor during ploughing, both on-land and within furrows. *Soil Tillage Res.* 68, 39–47.
- Keller, T., Défossez, P., Weisskopf, P., Arvidsson, J., Richard, G., 2007. SoilFlex: a model for prediction of soil stresses and soil compaction due to agricultural field traffic including a synthesis of analytical approaches. *Soil Tillage Res.* 93 (2), 391–411.
- Keller, T., Lamandé, M., Peth, S., Berli, M., Delenne, J.Y., Baumgarten, W., Rabbel, W., Radjai, F., Rajchenbach, J., Selvadurai, A.P.S., Or, D., 2013. An interdisciplinary approach towards improved understanding of soil deformation during compaction. *Soil Tillage Res.* 128, 61–80. <https://doi.org/10.1016/j.still.2012.10.004>.
- Kuhwald, M., Blaschek, M., Minkler, R., Nazemtseva, Y., Schwanebeck, M., Winter, J., Duttmann, R., 2016. Spatial analysis of long-term effects of different tillage practices based on penetration resistance. *Soil Use Manag.* 32 (2), 240–249. <https://doi.org/10.1111/sum.12254>.
- Lamandé, M., Schjønning, P., Tøgersen, F.A., 2007. Mechanical behaviour of an undisturbed soil subjected to loadings: effects of load and contact area. *Soil Tillage Res.* 97, 91–106.
- Lamandé, M., Schjønning, P., 2011. Transmission of vertical stress in a real soil profile. part iii: effect of soil water content. *Soil Tillage Res.* 114, 78–85.
- Lamandé, M., Schjønning, P., 2011. Transmission of vertical stress in a real soil profile. part ii: effect of tyre size, inflation pressure and wheel load. *Soil Tillage Res.* 114, 71–77.
- Lebert, M., Horn, R., 1991. A method to predict the mechanical strength of agricultural soils. *Soil Tillage Res.* 19 (2–3), 275–286.
- Lipiec, J., Szustak, A., Tarkiewicz, S., 1992. Soil compaction: responses of soil physical properties and crop growth. *Zeszyty Problemowe Postępów Nauk Rolniczych* 398, 113–117.
- Majdoubi, R., Masmoudi, L., Elharif, A., 2024. Analysis of soil compaction under different wheel applications using a dynamical cone penetrometer. *J. Terramechanics* 111, 21–30. <https://doi.org/10.1016/j.jterra.2023.09.001>.
- McPhee, J.E., Antille, D.L., Tullberg, J.N., Doyle, R.B., Boersma, M., 2020. Managing soil compaction – a choice of low-mass autonomous vehicles or controlled traffic? *Biosyst. Eng.* 195, 227–241. <https://doi.org/10.1016/j.biosystemseng.2020.05.006>.
- Mordhorst, A., Zimmermann, I., Peth, S., Horn, R., 2012. Effect of hydraulic and mechanical stresses on cyclic deformation processes of a structured and

- homogenized silty Luvis Chernozem. *Soil Tillage Res.* 125 (2012), 3–13. <https://doi.org/10.1016/j.still.2012.06.008>.
- Naderi-Boldaji, M., Kazemzadeh, A., Hemmat, A., Rostami, S., Keller, T., 2017. Changes in soil stress during repeated wheeling: a comparison of measured and simulated values. *Soil Res.* 56 (2), 204–214.
- Nolting, K., Brunotte, J., Lorenz, M., & Sommer, C., 2006. Bodenverdichtung: Bewegt sich was? - Setzungsmessungen im Unterboden unter hoher Radlast. *Agricultural engineering. Eu*, 61(4), 190–191. DOI: 10.1515/lt.2006.1093.
- O'Sullivan, M.F., Simota, C., 1995. Modelling the environmental impacts of soil compaction: a review. *Soil Tillage Res.* 35 (1–2), 69–84. [https://doi.org/10.1016/0167-1987\(95\)00478-B](https://doi.org/10.1016/0167-1987(95)00478-B).
- Patel, S.K., Mani, I., 2011. Effect of multiple passes of tractor with varying normal load on subsoil compaction. *J. Terramech.* 48 (4), 277–284. <https://doi.org/10.1016/j.tterra.2011.06.002>.
- Peters, A., Germer, K., Naseri, M., Rolfes, L., Lorenz, M., 2025. Modeling compaction effects on hydraulic properties of soils using limited information. *Soil Tillage Res.* 246, 106349.
- Peth, S., Horn, R., 2006. The mechanical behavior of structured and homogenized soil under repeated loading. *J. Plant Nutr. Soil Sci.* 169, 401–410. <https://doi.org/10.1002/jpln.200521942>.
- Peth, S., Rostek, J., Zink, A., Mordhorst, A., Horn, R., 2010. Soil testing of dynamic deformation processes of arable soils. *Soil Tillage Res.* 106, 317–328. <https://doi.org/10.1016/j.still.2009.10.007>.
- Pulido-Moncada, M., Munkholm, L.J., Schjønning, P., 2019. Wheel load, repeated wheeling, and traction effects on subsoil compaction in northern Europe. *Soil Tillage Res.* 186, 300–309. <https://doi.org/10.1016/j.still.2018.11.005>.
- Pytko, J., 2005. Effects of repeated rolling of agricultural tractors on soil stress and deformation state in sand and loess. *Soil Tillage Res.* 82 (1), 77–88. <https://doi.org/10.1016/j.still.2004.06.005>.
- Pytko, J., Dabrowski, J., Zajac, M., Tarkowski, P., 2006. Effects of reduced inflation pressure and vehicle loading on off-road traction and soil stress and deformation state. *J. Terramechanics* 43 (4), 469–485. <https://doi.org/10.1016/j.tterra.2005.06.001>.
- Ren, L., D'Hose, T., Ruysschaert, G., de Pue, J., Meftah, R., Cnudde, V., Cornelis, W.M., 2019. Effects of soil wetness and tyre pressure on soil physical quality and maize growth by a slur-ry spreader system. *Soil Tillage Res.* 195, 2019. <https://doi.org/10.1016/j.still.2019.104344>.
- Schjønning, P., Lamandé, M., 2018. Models for prediction of soil precompression stress from readily available soil properties. *Geoderma* 320, 115–125.
- Seehusen, T., Riggert, R., Fleige, H., Horn, R., & Riley, H., 2019. Soil compaction and stress propagation after different wheeling intensities on a silt soil in South-East Norway. *Acta Agriculturae Scandinavica, Section B—Soil & Plant Science* 69(4), 343–355.
- Seabold, S., Perktold, J., 2010. *Statsmodels: Econometric and Statistical Modeling with Python*. Proceedings of the 9th Python in Science Conference, 92–96. DOI: 10.25080/Majora-92bf1922-011.
- Soane, B. D., Van Ouwerkerk, C., 1994. Soil compaction problems in world agriculture. In *Developments in agricultural engineering* (Vol. 11, pp. 1–21). Elsevier. DOI: 10.1016/B978-0-444-88286-8.50009-X.
- Söhne, W., 1958. Fundamentals of pressure distribution and soil compaction under tractor tires. *Agri. Eng.* 39, 276–290.
- Startsev, A.D., McNabb, D.H., 2001. Skidder traffic effects on water retention, pore-size distribution, and van Genuchten parameters of boreal forest soils. *Soil Sci. Soc. Am. J.* 65 (1), 224–231. <https://doi.org/10.2136/sssaj2001.651224x>.
- Ten Damme, L., Schjønning, P., Munkholm, L.J., Green, O., Nielsen, S.K., Lamandé, M., 2021. Soil structure response to field traffic: effects of traction and repeated wheeling. *Soil Tillage Res.* 213, 105128. <https://doi.org/10.1016/j.still.2021.105128>.
- Tullberg, J., 2010. Tillage, traffic and sustainability—a challenge for ISTRO. *Soil Tillage Res.* 111 (1), 26–32. <https://doi.org/10.1016/j.still.2010.08.008>.
- Van den Akker, J.J.H., 2004. SOCOMO: a soil compaction model to calculate soil stresses and the subsoil carrying capacity. *Soil Tillage Res.* 79, 113–127.
- Zink, A., Fleige, H., Horn, R., 2010. Load risks of subsoil compaction and depths of stress propagation in arable luvisols. *Soil Sci. Soc. Am. J.* 74 (5), 1733–1742.
- Zink, A., Fleige, H., Horn, R., 2011. Verification of harmful subsoil compaction in loess soils. *Soil Tillage Res.* 114 (2), 127–134.